Journal of *Marine Science and Engineering*

MDPI

Article

Influence of Beach Slope on Morphological Changes and Sediment Transport under Irregular Waves

Sara Dionísio António [1], Jebbe van der Werf [1,2,*], Erik Horstman [1], Iván Cáceres [3], José Alsina [3], Joep van der Zanden [4] and Suzanne Hulscher [1]

[1] Faculty of Engineering Technology, University of Twente, P.O. Box 217, 7500 AE Enschede, The Netherlands; s.dionisioantonio@utwente.nl (S.D.A.); e.m.horstman@utwente.nl (E.H.); s.j.m.h.hulscher@utwente.nl (S.H.)
[2] Unit of Marine & Coastal Systems, Deltares, P.O. Box 177, 2600 MH Delft, The Netherlands
[3] Laboratori d'Enginyria Marítima, Universitat Politècnica de Catalunya, C. Jordi Girona 1–3, 08034 Barcelona, Spain; i.caceres@upc.edu (I.C.); jose.alsina@upc.edu (J.A.)
[4] Offshore Department, Maritime Research Institute Netherlands (MARIN), P.O. Box 28, 6700 AA Wageningen, The Netherlands; j.v.d.zanden@marin.nl
* Correspondence: j.j.vanderwerf@utwente.nl

Abstract: This paper presents new data from large-scale wave flume experiments. It shows the beach profile evolution and sediment transport for two different bed slopes (1:15 and 1:25), and three irregular high-energy erosive wave conditions and one low-energy accretive wave condition. The bulk cross-shore net sediment transport was investigated for the total active profile and for the surf and swash zone separately. It is shown that the steep slope is morphologically more active than the gentle slope, with faster and more pronounced morphological changes and larger sediment transport rates. For both slopes, the total and surf zone net sediment transport were offshore-directed for erosive waves and onshore-directed for the accretive wave condition. However, the net swash zone transport for the erosive wave conditions was offshore-directed for the steep slope and onshore-directed for the gentle slope. The direction and magnitude of the total and surf zone sediment transport correlate well with the slope-corrected Dean criterion with increasing offshore-directed sediment transport (erosion) observed for increasing wave energy and bed slope. This relation does not hold for the swash zone sediment transport along the gentle slope, suggesting that swash zone sediment transport processes are not well captured when using a simple predictor such as the (modified) Dean number. Differences in sediment transport in the swash for the different slopes are likely influenced by differences in incoming wave energy, wave–swash interactions and the relative importance of long- and short-waves.

Keywords: beach morphology; sediment transport; large-scale wave flume experiments; swash zone; surf zone; irregular waves

Citation: Dionísio António, S.; van der Werf, J.; Horstman, E.; Cáceres, I.; Alsina, J.; van der Zanden, J.; Hulscher, S. Influence of Beach Slope on Morphological Changes and Sediment Transport under Irregular Waves. *J. Mar. Sci. Eng.* **2023**, *11*, 2244. https://doi.org/10.3390/jmse11122244

Academic Editor: Achilleas Samaras

Received: 12 October 2023
Revised: 16 November 2023
Accepted: 24 November 2023
Published: 27 November 2023

1. Introduction

Natural beaches have an equilibrium morphology that is determined by the interplay between their grain size and the prevailing wave climate. Any changes in the wave forcing induce morphological changes as a consequence of the beach readjustment to this new condition. In the last few years, the influence of the hydrodynamics on the morphological developments and sediment transport in the surf and swash zone have received increasing attention [1–8]. Studies have demonstrated that under high-energy erosive waves the overall net sediment transport of the beach is offshore-directed, resulting in offshore bar migration and shoreline retreat. Conversely, under low-energy accretive waves the net onshore-directed sediment fluxes cause onshore bar migration and shoreline accretion [2,4]. However, under the same wave forcing differences in sediment transport between the surf and swash zones [9,10] and within the swash zone may occur [11,12].

Wave breaking induces large amounts of turbulence that enhance sediment entrainment from the bed. This process depends on the characteristics of the breaking wave, with plunging breakers being more efficient in sediment stirring and mobility than spilling breakers [13]. The wave breaking-induced turbulence in the surf zone can be injected into the swash zone and advected by the swash front with the turbulent face in contact with the bed which promotes local sediment stirring [14,15]. This turbulence depends on the bore height, local water depth, and wave dissipation [15,16], which in turn are directly related to the beach slope [17,18]. For steeper beaches, with narrower and deeper surf and swash zones, higher bore turbulence is expected due to the spatial concentration of energy dissipation from plunging breakers, contributing to higher suspended sediment concentrations [15].

The overall time-averaged direction and magnitude of the net sediment transport in the swash zone under irregular waves is determined by the occurrence of a small number of larger erosive/accretive events that disturb the normally distributed net bed level changes [19–21]. The erosive/accretive nature of a single swash event has been attributed to a combination of several processes such as sediment advection [22], interactions between the surf and swash zone [18,23–25], or local wave–swash interactions occurring in the outer swash [23,25–27].

Wave–swash interactions occur when the incident bore interacts with the preceding swash event. Three main types of wave–swash interactions are generally considered, for example [24]:

1. Wave capture. The second wave captures the previous one; both are in the uprush stage.
2. Weak wave–backwash interaction. The uprush of the second wave overruns the backwash of the previous one.
3. Strong wave–backwash interaction. This is similar to type 2, but now the backwash is stronger than the incoming uprush. This results in a stationary bore and the resulting flow is offshore-directed.

All wave–swash interaction types produce high levels of turbulence that increase the sediment stirring and mobility [26]. Cáceres and Alsina [26] have found that strong wave–backwash interactions tend to result in erosion events, while weak wave–backwash interactions and wave capture events tend to induce accretion. The dominant spectral band of the waves in the swash zone and the phase of the short waves within the group influence the amplitude of the swash motions and the dominant type of wave–swash interactions [25,28]. The degree of wave–swash interactions can be quantified by the ratio of the natural period of individual swash events T_s and the incident wave period T through the parameter $\hat{T} = T_s/T$ [25]. For $\hat{T} < 1$ little or no interactions occur, while the degree/number of wave–swash interactions increases as $\hat{T}$ increases.

Only a limited number of studies have investigated the influence of the beach slope on sediment transport in the surf and swash zone [12,20,23,29,30]. Studies have demonstrated that on intermediate beaches, characterized by steeper slopes, the sediment transport is dominated by incident short waves with a relatively high numbers of uprushes and backwashes resulting in relatively high suspended sediment concentrations. Conversely, on dissipative beaches, characterized by a gentle slope, the sediment transport in the swash is infragravity-dominated. This leads to lower suspended sediment concentrations, as the transfer of energy from the incident wave band to the infragravity band results in a reduction in the number of uprushes passing over the bed [12]. Furthermore, Alsina et al. [23] showed that the number of wave–swash interactions is slope-dependent, as well as the magnitude and frequency of large backwashes. For a gentler sloping, more dissipative beach, there is an increase in the number of wave–swash interactions. At the same time, the magnitude and frequency of large backwashes (responsible for strong wave–backwash interaction) are reduced, leading to a reduction of offshore suspended sediment transport.

Previous studies have shown that simple wave and beach parameters can be used to predict the tendency of a beach to erode or accrete due to wave-induced cross-shore

sediment transport [31–36]. The Dean parameter [32] is a widely used parameter that relates the offshore wave forcing with a sediment-related descriptor:

$$\Omega_D = \frac{H_0}{w_s T_p}, \tag{1}$$

where H_0 is the offshore (significant) wave height, T_p is the peak wave period and w_s is the sediment settling velocity. Values of $\Omega_D < 3.2$ indicate beach accretion and values $\Omega_D > 3.2$ indicate erosion [36]. Later, a slope-corrected version of the Dean's parameter was developed by Hattori and Kawamata [33] in order to include the effect of the beach slope on the net sediment transport in the surf:

$$\Omega_{HK} = \frac{H_0}{w_s T_p} \tan\beta, \tag{2}$$

where β is the beach slope. According to Hattori and Kawamata [33], for $\Omega_{HK} < 0.08$ onshore-directed transport dominates and for $\Omega_{HK} > 0.08$ offshore-directed transport dominates, and a mix region is found between $0.05 < \Omega_{HK} < 0.11$. Although these criteria have been widely applied to predict erosion/accretion in the surf zone, the applicability of these criteria in the swash zone has yet to be investigated.

Large-scale laboratory experiments are well-suited to investigate beach morphodynamics and sediment transport under controlled and repeatable conditions. However, previous large-scale laboratory experiments that investigated sediment transport and morphodynamics all considered relatively steep slopes (1:15 is a commonly used slope [2,26,37,38]). The extent of the influence of a gentler slope on the swash zone sediment transport and morphodynamics, as well as its impact on the swash–surf interactions have not been thoroughly investigated yet.

The aim of this study is to obtain a quantitative understanding of the effect of the bed slope on beach morphology evolution and sediment transport in the surf and swash zone, for both erosive and accretive wave conditions. These effects are investigated through real-scale experiments with a "standard" bed slope of 1:15 and a gentler 1:25 slope, with identical sediment size. These slopes are exposed to a series of irregular wave conditions.

This paper first describes the experimental set-up, data-processing, and data analysis in Section 2. Results of the beach morphology, sediment transport, and hydrodynamics are presented in Section 3 and discussed in Section 4. The conclusions follow in Section 5.

2. Experiments

2.1. Experimental Set-Up

The experiments were conducted in the large-scale CIEM wave flume at the Universitat Politècnica de Catalunya (UPC, Barcelona, Spain) as part of the Shaping the Beach project The CIEM flume is 100 m long, 3 m wide, and 4.5 m deep (Figure 1). Two sets of experiments were conducted with different initial beach slopes. The horizontal x-coordinate has its origin at the initial shoreline and is negative towards the wave paddle (offshore) and positive towards the beach face (onshore) (see Figure 2). The still water depth h_0 was 2.47 m. One set started with an initial 1:15 slope, similar to previous experiments in this flume [1,26,37]. The second set of experiments started with an initial 1:25 slope. The 1:25 slope had a steeper 1:10 slope beach face offshore of the maximum depth of closure to be able to fit the gentle beach slope in the flume (Figure 2). In both cases, the bed consisted of well-sorted medium sand with grain diameters d_{50} = 0.25 mm, d_{10} = 0.15 mm, and d_{90} = 0.37 mm, and a measured mean settling velocity w_s = 0.034 m/s. Following Baldock et al. [3], two dividers were added on the upper beach to reduce cross-flume flows and bed asymmetries in the swash zone (Figure 1). The dividers consisted of two (three) metal plates in the 1:15 (1:25) slope of 3 mm width, 0.70 m high, 3 m long, buried approximately 0.40 m into the initial bed (extending approximately 0.30 m above the initial bed). The dividers were positioned between approximately x = 0.60 m and x = 6.60 m for the

1:15 slope and x = 0.95 m and x = 9.95 m for the 1:25 slope dividing the flume in three parts of similar width (approximately 0.90 m on the sides and 1.2 m in the middle because of instrument positioning).

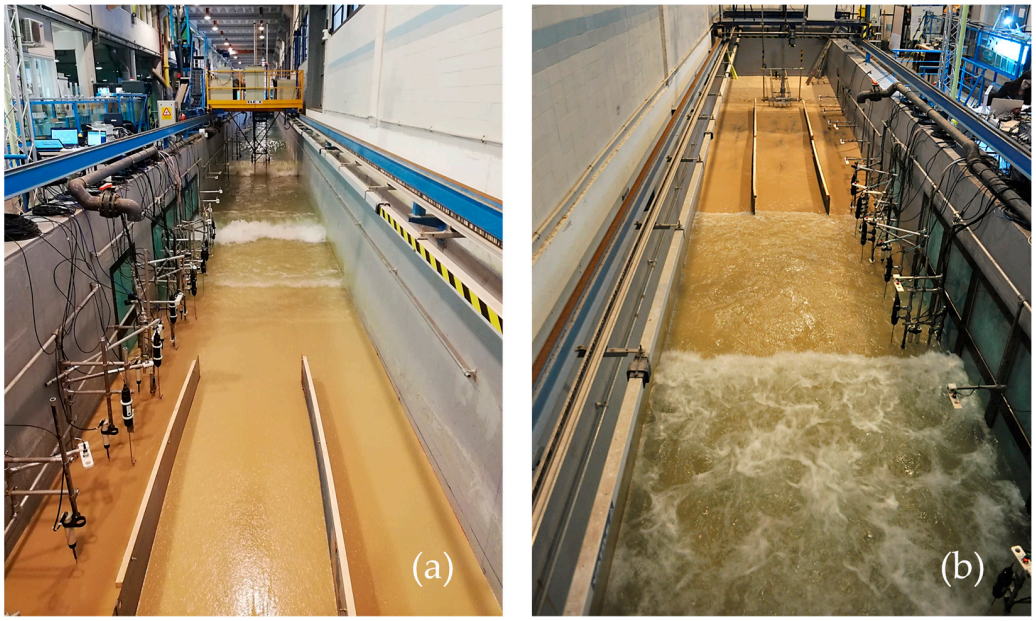

Figure 1. Experimental set-up in the large-scale CIEM wave flume at the Universitat Politècnica de Catalunya: (**a**) view down the beach towards the wave paddle and (**b**) view towards the beach.

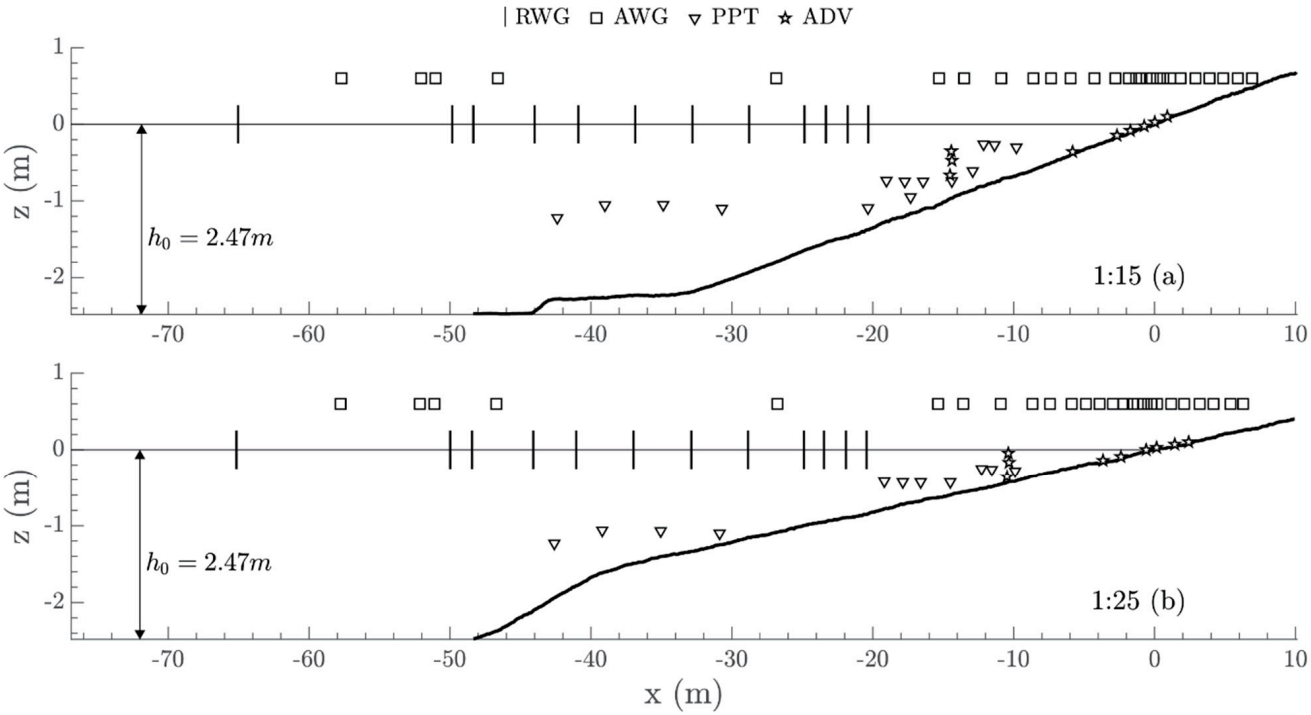

Figure 2. Experimental set-up: (**a**) initial 1:15 slope and (**b**) initial 1:25 slope. The water levels were measured by resistive wave gauges (RWGs, vertical black lines), acoustic wave gauges (AWGs, squares) and pressure transducers (PPTs, triangles). Velocities were measured with acoustic Doppler velocimeters (ADVs, stars).

2.2. Wave Conditions

The waves were generated at intermediate water depth by the wedge-type wave maker. A sequence of irregular wave conditions was generated for each bed slope. Tables 1 and 2 summarize the wave conditions in each series, including the target offshore significant wave height H_s, the peak period T_p, Jonswap spectrum with peak enhancement factor γ, the Dean parameter Ω_D, the slope corrected Dean parameter Ω_{HK}, and the surf similarity parameter or Iribarren number ξ_0 for corresponding deep water wave height H_0. After building each hand-made bed profile, the profile was exposed to a Benchmark (B) wave for 15 min (176 individual waves) in order to compact the bed. The first sequence (Table 1) started from the 1:15 slope and consisted of a series of three consecutive increasing wave energy waves (E1, E2, and E3) interrupted by a low-energy wave (A1) after the first energetic wave (E1). The second sequence (Table 2) started from the hand-made 1:25 slope and consisted of a series of three consecutive increasing wave energy waves (E1, E2, and E3) followed by the low-energy wave (A1). In contrast to the wave sequence on the 1:15 slope, the low-energy accretive wave condition (A1) on the 1:25 slope was moved to the end of the sequence because of the slow morphological development observed during the first erosive wave condition (E1). Each high-energy wave condition was run for a total of 180 min (except for E3 on the 1:25 slope that ran for a total of 210 min) in runs of 30 min (611 individual waves) and the low-energy wave condition was run for 600 min in runs of 60 min (896 individual waves).

Table 1. Wave sequence for 1:15 slope.

Wave Condition		H_s (m)	T_p (s)	γ (−)	Ω_D (−)	Ω_{HK} (−)	ξ_0 (−)	Time (min)
B	Benchmark	0.42	4.0	3.33	3.31	0.22	0.43	15
E1	High energy 1	0.45	3.5	3.33	4.12	0.27	0.42	180
A1	Low energy 1	0.25	5.2	1.33	1.42	0.09	0.58	600
E2	High energy 2	0.55	3.5	3.33	5.04	0.34	0.38	180
E3	High energy 3	0.65	3.5	3.33	5.95	0.39	0.35	180

Table 2. Wave sequence for 1:25 slope.

Wave Condition		H_s (m)	T_p (s)	γ (−)	Ω_D (−)	Ω_{HK} (−)	ξ_0 (−)	Time (min)
B	Benchmark	0.42	4.0	3.33	3.31	0.13	0.39	15
E1	High energy 1	0.45	3.5	3.33	4.12	0.16	0.37	180
E2	High energy 2	0.55	3.5	3.33	5.04	0.06	0.34	180
E3	High energy 3	0.65	3.5	3.33	5.95	0.20	0.31	210
A1	Low energy 1	0.25	5.2	1.33	1.42	0.24	0.52	600

2.3. Measurements and Data Treatment

The water surface elevation was measured by 13 resistive wave gauges (RWG), 26 acoustic wave gauges (AWG), and 14 pressure sensors (PPT). These were deployed along the full extension of the flume, from the deeper part to the high end of the beach (Figure 2). All water level measurements were obtained at a sampling frequency of 40 Hz. The wave gauge and pressure measurements were vertically referenced with respect to the still water level. In the swash zone, the AWGs measured the water surface elevation when the bed was submerged, and the bed level when exposed. The measurement accuracy of the RWGs and PPTs placed seaward of the shoreline is estimated to be about 1 mm. Three different AWGs were deployed in the study area with long, medium, and short vertical ranges of 2.3, 1.3 and 0.3 m, respectively. The long-range AWGs (with a 1 mm accuracy according to the manufacturer) were deployed in the deeper part of the profile and shoaling region up to $x = -7$ m (Figure 2). The medium range AWGs were deployed in the surf and swash zones between $x = -7$ and $x = 3$ m, while the short-range AWGs (with a 0.025 mm accuracy

according to the manufacturer) were deployed in the upper swash from x = 3 m up to the end of the measured bed profile. The AWG measurements were de-spiked. Subsequently, a low-pass filter with a cut-off frequency 8 Hz was applied to eliminate spurious electronic noise contributions [27]. The water level was retrieved from the pressure measurements by the non-linear, weakly dispersive approach by Bonneton et al. [39] using a low-pass filter with a cut-off frequency of $4.5/T_p$ Hz.

The water surface elevation measurements were decomposed in the mean ($\overline{\eta}$), long-wave (η_l), and incident short (η_s) wave components by applying a low-pass filter with a cut-off frequency of half the deep water peak frequency ($f_{split} = 0.5 f_p$) [40]:

$$\eta = \overline{\eta} + \eta_l + \eta_s. \tag{3}$$

Furthermore, the crest-to-through asymmetry or wave skewness Sk and wave asymmetry As indicators of onshore/offshore bottom fluxes—and thus, sediment transport—are calculated from the time series of surface elevation [6]:

$$Sk = \frac{\left\langle (\eta - \overline{\eta})^3 \right\rangle}{\left\langle (\eta - \overline{\eta})^2 \right\rangle^{3/2}} \text{ and} \tag{4}$$

$$As = \frac{\left\langle \mathcal{H}^3(\eta - \overline{\eta}) \right\rangle}{\left\langle (\eta - \overline{\eta})^2 \right\rangle^{3/2}}, \tag{5}$$

where $\mathcal{H}$ denotes the Hilbert transform. A standing wave (seiche) was generated in the flume with a period of 40–50 s (0.02–0.025 Hz), corresponding to the flume natural resonance period. The seiching amplitudes are with ~0.01 m significantly smaller than the amplitudes at the short-wave peak (0.2–0.3 Hz) and long-wave frequency (0.05–0.1 Hz) band width of ~0.2 m and ~0.1 m, respectively. As a result, the seiche orbital velocities are an order of magnitude smaller than the short- and long-wave velocities. Furthermore, the correlation between seiche orbital velocities and sand suspension is weak. Hence flume-seiching does not lead to a significant net sand transport contribution.

Between each run, bed levels were measured by a mechanical profiler in still water conditions. These profiler measurements were done along the centerline of the flume, measuring the emerged and submerged bed with a spatial resolution of Δx = 0.02 m and a vertical accuracy of 0.01 m. The run-up and run-down limits were obtained by visual observations during each run and confirmed by video recordings and AWG measurements.

2.4. Profile Definitions

Beach parameters such as the shoreline, breaker bars, and berm are indicators of the profile evolution [3,41]. Each parameter was identified for each measured profile as shown in Figure 3. The shoreline location x_s is the cross-shore location at which the still water level (SWL) intersects with the bed. The erosion (or recovery) of the shoreline is determined by the cross-shore difference between two consecutive shoreline positions. In a double-bar system, the main (outer) breaker bar crest is defined as the maximum height difference (z_{Mbar}) between the initial profile and the studied profile (seaward from the shoreline) with cross-shore coordinate x_{Mbar}. The main bar area A_{Mbar} is found via the integration between the initial and the studied profile delimited by its length, defined by the distance between the points at which the profiles intersect. Similarly, the secondary (inner) bar is defined as the largest difference (z_{Sbar}) between the two bed profiles for the section between the main breaker bar and the shoreline (x_{Sbar}). The main bar is generally defined as the "active" bar where most waves break [4] which is generally of larger size and located seaward compared to the secondary bar. In a single-barred system, there is only a main trough in-between the main bar and the beach with no secondary bar. Landward from the shoreline a berm

location x_{Berm} is defined as the maximum difference z_{Berm} between the initial profile and the studied profile.

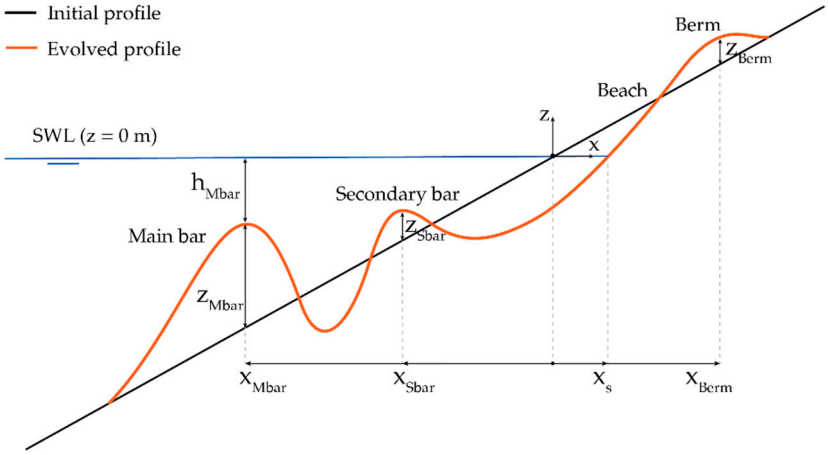

Figure 3. Definition of the morphological parameters used in this study.

2.5. Sand Transport

The time-averaged sand transport rate $q_s(x)$ was obtained from the bed level change Δz over the corresponding time interval Δt using the mass balance equation [2]:

$$q_s(x_i) = q_s(x_{i-1}) - \int_{x_{i-1}}^{x_i} (1 - \varepsilon_p) \frac{\Delta z_i}{\Delta t} dx, \quad (6)$$

where ε_p = 0.36 the porosity of loosely packed sand. Based on the assumption that no sediment transport occurs past the active profile, Equation (6) is applied for the profile between the depth of closure x_{min}, and the run-up limit, x_{max}. The depth of closure is defined as the most offshore location where no significant bed level change is observed. Following the correction methodology by Baldock et al. [3], the remaining closure error was distributed uniformly along the profile. Negative and positive values of q_s represent offshore- and onshore-directed sediment transport rates, respectively.

The beach response (erosive or accretive) was categorized using the bulk cross-shore sediment transport Q_s over a time interval, and Q_s (m^3) is determined from integrating q_s along the profile between the same closure limits [3,42]:

$$Q_s = \Delta t \int_{x_{min}}^{x_{max}} q_s(x) dx. \quad (7)$$

Positive values of Q_s indicate net shoreward sediment movement (accretion), and negative values indicate net offshore movement (erosion).

To investigate the bulk sediment transport Q_s within different nearshore zones, the active profile was divided in two main zones: the swash and surf zone. The swash zone includes the outer swash region, where wave–swash interactions occur, and the inner swash region, where pure swash motions occur. By definition, the sediment transport in the outer swash is influenced not only by the wave–swash interactions but also by occasional inner surf processes due to the irregularity of the wave forcing [29]. The swash zone was defined as the cross-shore area between the maximum run-up limit and the minimum backwash limit (minimum offshore location where the backwash encounters the incoming bore). The surf zone, for the sake of simplification, includes the remaining nearshore zone where there is sediment movement due to wave shoaling and breaking. Consequently, the surf zone was defined as the cross-shore area between the swash limit and the depth of closure, x_{min}. The sediment transport Q_s was calculated for the total active profile ($Q_{s,tot}$) as well as for the surf ($Q_{s,surf}$) and swash ($Q_{s,swash}$) zones separately.

In the analyses below, we assume the beach to be in a so-called quasi-equilibrium state when the bed level changes are relatively small after large initial adjustments. This is reflected in a fully developed bar and beach profile that still shows some minor change of the bar and shoreline position. Cumulative bulk sediment transport rates tend towards a constant value in this quasi-equilibrium state [3,4].

3. Results

3.1. Beach Profile Evolution

3.1.1. General Observations

The beach profile evolution for the initial slopes of 1:15 and 1:25 is shown in Figure 4. The figure includes the profiles at the end of each wave condition (Figure 4a,c) and time-stacks of elevation changes Δz_0 (Figure 4b,d). The time-stack plots also mark the shoreline (black solid line), the crest of the main bar (filled circles), the crest of the secondary bar (empty circles), and the crest of the berm (black diamonds).

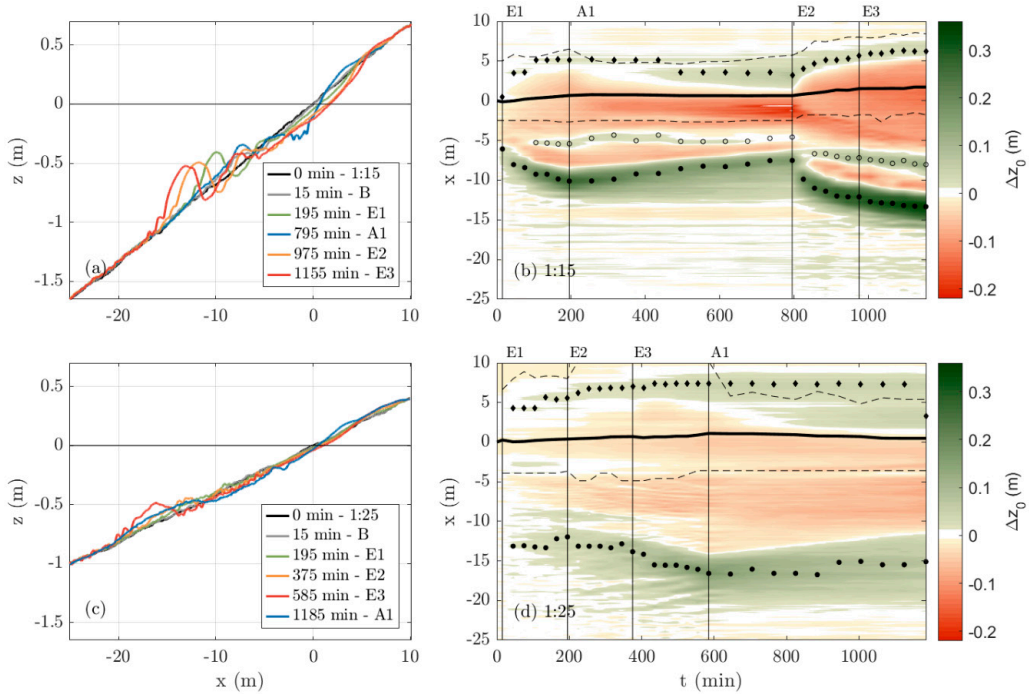

Figure 4. Profile evolution for (**a**,**b**) the 1:15 slope and (**c**,**d**) the 1:25 slope, both exposed to similar sequences of wave conditions (see Tables 1 and 2): (**a**,**c**) profiles at the end of each wave condition and (**b**,**d**) time-stacks of elevation changes Δz_0 from the initial profile over time. The shoreline (black solid line) and the crests of the (main) breaker bar (filled circles), the secondary breaker bar (empty circles, only for the 1:15 slope), and the berm (solid diamonds) and the swash limits (dashed black line) are indicated.

The beach development for the steeper slope is characterized by the development of a well-defined main and secondary bar during the first energetic condition E1, accompanied by deepening of the beach face with the retreat of the shoreline and appearance of a berm. These features become more accentuated with increasing wave energy, with the biggest difference between the initial slope and the obtained profile seen at the end of the highest wave energy condition E3 over the main bar (Δz_0 = 0.36 m). The interruption of the high wave energy sequence by a lower-energy wave A1 induced a break in the erosive development of the steeper profile. During this wave condition, the main bar reduced in size accompanied by the near extinction of the secondary bar. This was accompanied by a strong deepening of the inner swash and berm growth, producing a difference between the initial slope and the profile at the end of A1 of $\Delta z_0 = -0.21$ m in the inner swash and Δz_0 = 0.07 m over the berm.

The profile is seen morphologically active between approximately $x = -18$ m to $x = 9$ m and $x = -14$ m to $x = 7$ m for the higher and lower energy wave conditions, respectively. The overall beach development for the 1:15 slope is in accordance with observations from previous studies for the same slope and grain size and similar wave conditions [1,4,26].

On the other hand, the morphological development of the gentler slope during the higher wave energy conditions was characterized by the development of a single flat bar accompanied by deepening of both the trough and shoreface and berm growth. Similar to the steeper slope, these features' growth followed the increase in wave energy reaching their maximum growth by the end of E3 with $\Delta z_0 = 0.18$ m over the bar. During the low-energy wave condition A1, the bar flattened out followed by deepening of the trough and inner swash and recovery of the beach accompanied by berm growth. Again, the trough/inner swash and the berm reached their maximum deepening/growth by the end of A1 with $\Delta z_0 = -0.08$ m and $\Delta z_0 = 0.06$ m, respectively. Furthermore, the profile on the gentler slope is morphologically active between approximately $x = -22$ m to the end of the flume at $x = 10$ m for all wave conditions as opposed to the shorter active profile seen for the steeper slope.

Another characteristic that contrasts between the two sequences is the occurrence of perturbations in the profiles. The profile development for the 1:15 slope shows distinct small ripples only in the bar troughs between the two well-defined bars (mainly in the secondary bar trough), whereas the profiles for the 1:25 slope show the presence of ripples in both the bar and trough region. The breaker bar and shoreline evolution are studied in more detail in the subsequent sections.

3.1.2. Breaker Bar

In the following we discuss the main bar for the 1:15 bed slope cases and the single bar present during the 1:25 bed slope cases, which we refer to as "bar". In the present study, the stepwise increase in wave energy (E1, E2 and E3) for both slopes lead to the generation and growth of a (main) bar that progressively migrates offshore (Figure 5). These observations are in agreement with the tendency for offshore sandbar migration towards an equilibrium location for increasing wave heights [43]. However, the rates of bar development and migration are different for each slope. For the steeper slope, the main bar evolves rapidly, reaching a well-defined shape in the early stage of condition E1 and continues to grow at a steady rate while the wave energy increases (Figure 5c,d). This bar development is accompanied by the offshore migration in all high-energy conditions reaching a final position of $x = -10.1$ m, $x = -12.1$ m, and $x = -13.3$ m for E1, E2, and E3, respectively (Figure 5a). This offshore migration was accompanied by an increasing water depth above the bar for E2 and E3, reaching depths of $h_{Mbar} = 0.50$ m and $h_{Mbar} = 0.53$ m at the end of these conditions, respectively (Figure 5b). The offshore migration during the first 90 min of E1 and E2 is fast compared to the observed migration for E3. This increase in the migration rate at the beginning of a wave condition is related to how far the profile is from its morphological equilibrium state. For energetic conditions, beach profiles tend to change quickly in case of a larger disequilibrium [44]. On the steeper slope, the E1 case starts from a smooth slope and E2 starts after a beach recovery under the low-energy A1 wave condition. Both initial profiles are further away from the equilibrium states for the respective wave conditions than the profile at the beginning of wave condition E3. In all high energetic wave conditions on the steeper beach, the breaker bar reaches a quasi-equilibrium position after approximately 90 min, where the change in bar location between consecutive runs becomes minimal.

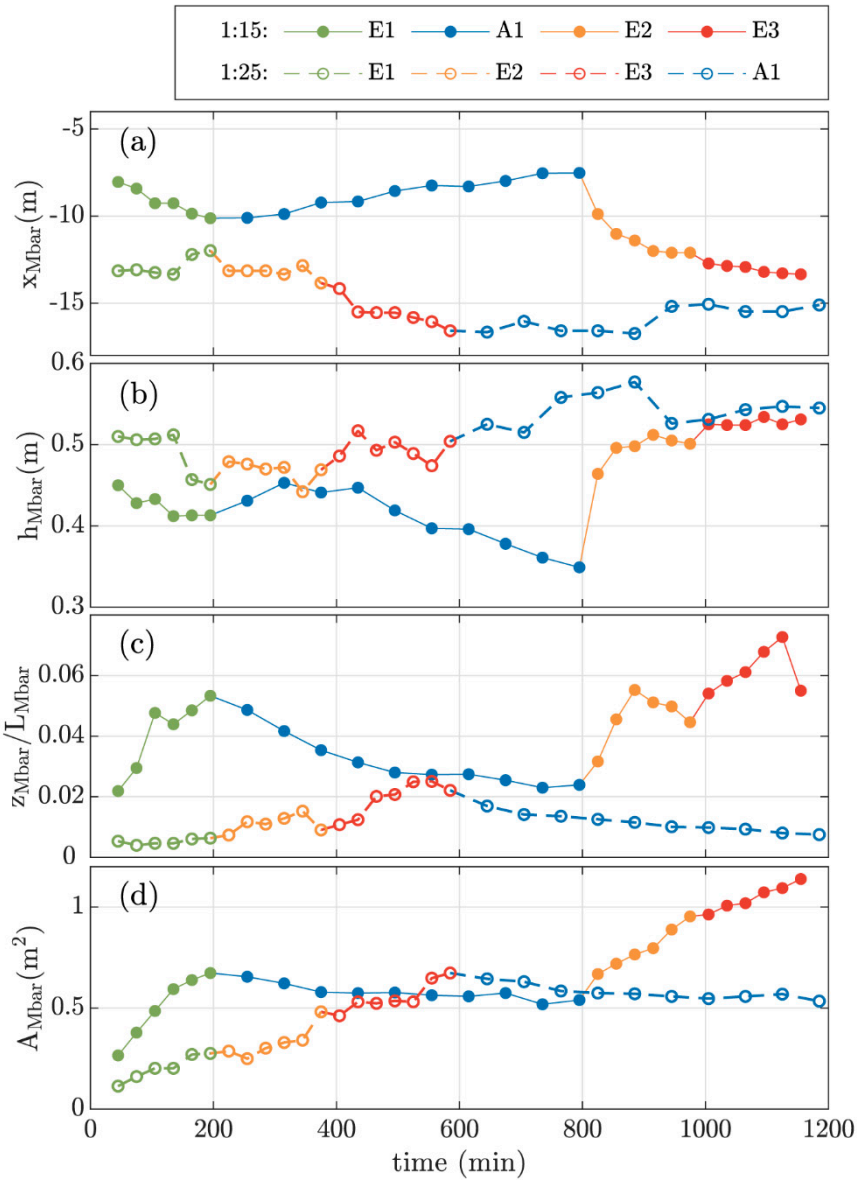

Figure 5. Main bar evolution over time for both slopes: (**a**) cross-shore location of the main bar crest x_{Mbar}, (**b**) water depth above the main bar crest h_{Mbar}, (**c**) main bar steepness z_{Mbar}/L_{Mbar} and (**d**) total area of the main bar A_{Mbar}. Note that there was only a single bar for the 1:25 bed slope cases.

On the other hand, on the gentler slope the bar starts to emerge as a wide shallow bar during condition E1 and only starts to gain substantial height during condition E2 (Figure 5c,d). Moreover, the bar for the 1:25 slope remains approximately at the same cross-shore location during E1 and E2 at approximately x = 13.2 m, starting its offshore migration only after it reached a considerable height during condition E2 (approximately at t = 375 min—note that the variability of bar location for condition E1 is the result of the development of perturbations in the bed and not attributed to bar migration) (Figure 5a,c,d). By the end of E2, the bar reached a position of $x = -13.8$ m, reaching its maximum offshore position at the end of E3 at $x = -16.6$ m. Due to the growth of the bar while at the same location, the water depth above the bar for condition E1 and E2 decreased, being approximately h_{Mbar} = 0.45 m and h_{Mbar} = 0.47 m at these conditions, respectively. The water depth slightly increased upon the offshore migration during E3 reaching h_{Mbar} = 0.50 m.

For the 1:25 slope the bar was first detected at about $x = -13$ m, i.e., about 5 m further offshore than the bar generated in the 1:15 slope at $x = -8.0$ m. For both slopes the (main) bar reached its maximum offshore location by the end of the highest wave

energy condition E3, at $x = -13.3$ m on the 1:15 slope and at $x = -16.6$ m for the 1:25 slope (Figure 5a). On the gentler slope, the bar thus reached its maximum offshore location about 3 m further offshore for 1:15 slope. The latter had approximately double the area ($A = 1.14$ m^2 for the 1:15 slope and $A = 0.67$ m^2 for the 1:25 slope) and a significantly more pronounced shape compared to the bar on the gentler slope (Figure 5c,d). Additionally, the water depth above the (main) bar on both slopes is similar, varying about 0.03 m between the main bars ($h_{Mbar} = 0.53$ m for the 1:15 slope and $h_{Mbar} = 0.50$ m for the 1:25 slope; Figure 5b).

During the low-energy accretive wave condition (A1) the (main) bars for both slopes have the same overall onshore migration tendency. However, this tendency displays different dynamics. For the 1:15 slope the main bar continuously migrated onshore reaching a final position of $x = -7.5$ m while slowly decreasing in height (Figure 5a,c). Due to the fast initial decrease in bar height, the water depth above the main bar crest first slightly increases to then be reduced by approximately 0.1 m due to the onshore migration of the bar (Figure 5b). In contrast, for the 1:25 slope the bar remains at its overall offshore position at $x = -16.6$ m in the first 300 min while slowly flattening out, after which it migrates onshore reaching $x = -15.1$ m by the end of condition A1 (Figure 5a,c). Due to this initial bar height reduction while maintaining its overall offshore position, the water depth above the crest increases from $h_{Mbar} = 0.5$ m to $h_{Mbar} = 0.6$ m (Figure 5b). Although the onshore migration and the evolution of the bar shape are not equivalent for both slopes, the changes of the area of the bar are about the same throughout the entire A1 condition reaching a similar final area of $A = 0.53$ m^2 (Figure 5d).

3.1.3. Shoreline Evolution

The relative cross-shore shoreline position x_s is an indicator of beach accretion/erosion (Figure 6). For both slopes the shoreline has the same overall tendency: erosion during the high-energy erosive wave conditions (E1, E2 and E3) and accretion during the low-energy accretive wave condition (A1). However, the shoreline change rates differ for each slope and wave condition.

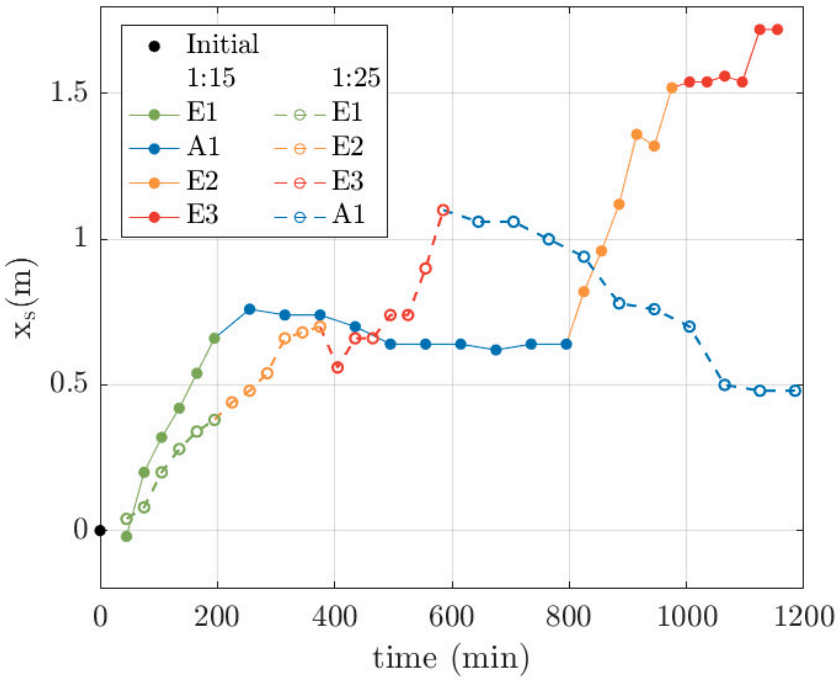

Figure 6. Shoreline location over time, relative to its initial position, for both slopes.

The shoreline position during the high-energy waves for the 1:15 slope evolves in a opposite pattern than the main bar position during these conditions, with the shore-

line progressively moving landward. For this slope, the shoreline final location was at x = 0.66 m, x = 1.52 m and x = 1.72 m for condition E1, E2 and E3, respectively. The largest shoreline erosion occurred during E1 and E2, eroding approximately 0.7 m and 0.9, respectively, and the smallest during E3, eroding 0.2 m. This suggests that, as for the main bar, the shoreline was closer to its equilibrium position for the E3 condition compared to E1 and E2 [44,45]. On the other hand, the shoreline final location for the high-energy wave conditions on the gentler slope was at x = 0.38 m, x = 0.70 m, and x = 1.10 m for condition E1, E2, and E3, respectively, resulting in a more or less steady shoreline erosion of approximately 0.3 to 0.4 m during each wave condition. The maximum cumulative shoreline retreat occurred at the end of wave condition E3 for both slopes, with the final location of the shoreline on the steeper slope being about 0.7 m further onshore than on the gentler slope.

During the low-energy wave condition A1, the shoreline advanced for both slopes (Figure 6), while the (main) bar migrated offshore (Figure 5a). The largest shoreline advance of about 0.6 m occurred on the gentler slope with the shoreline reaching x = 0.48 m after the beach recovered from erosion by the previous condition E3. For the steeper slope, the shoreline firstly slightly retreats about 0.1 m in the first 60 min of the low-energy wave condition, then slightly advances, and maintains a similar initial position of x = 0.64 m. Nevertheless, the final shoreline position for both slopes is close to each other, differing by about 0.15 m only.

The shoreline position at the end of each wave condition is presented against the Dean and the slope-corrected Dean parameters (Figure 7). Large Ω_D numbers correspond to more shoreline retreat; however, the Dean number poorly represents the effect of the beach slope on shoreline retreat/advance (Figure 7a). On the other hand, Ω_{HK} adequately captures the increased erosion and decreased accretion for increasing beach gradients under the same wave condition (Figure 7b), except for high wave condition E3 due to the initial condition (see Section 3.2).

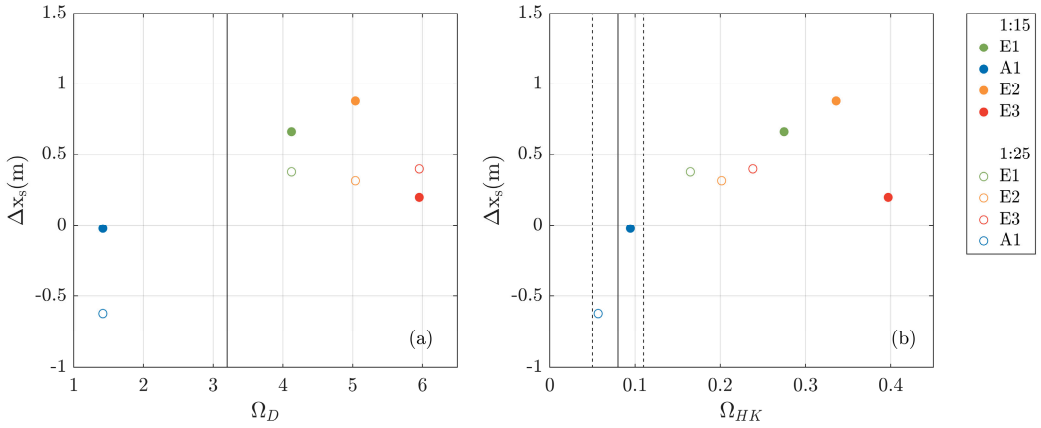

Figure 7. Movement of the shoreline position during each wave condition (negative = accretion; positive = erosion), for both slopes against the Dean parameter Ω_D (**a**) and the slope corrected version Ω_{HK} (**b**). The solid line represents the limits between accretion/erosion for both criteria (mix region within dashed lines).

3.2. Sediment Transport

The evolution of bulk sediment transport for the total profile and separated bulk transport for the surf and swash are presented in Figure 8. The cumulative Q_s is computed based on the profile at the beginning of each wave condition for the active profile (from depth of closure to run-up limit).

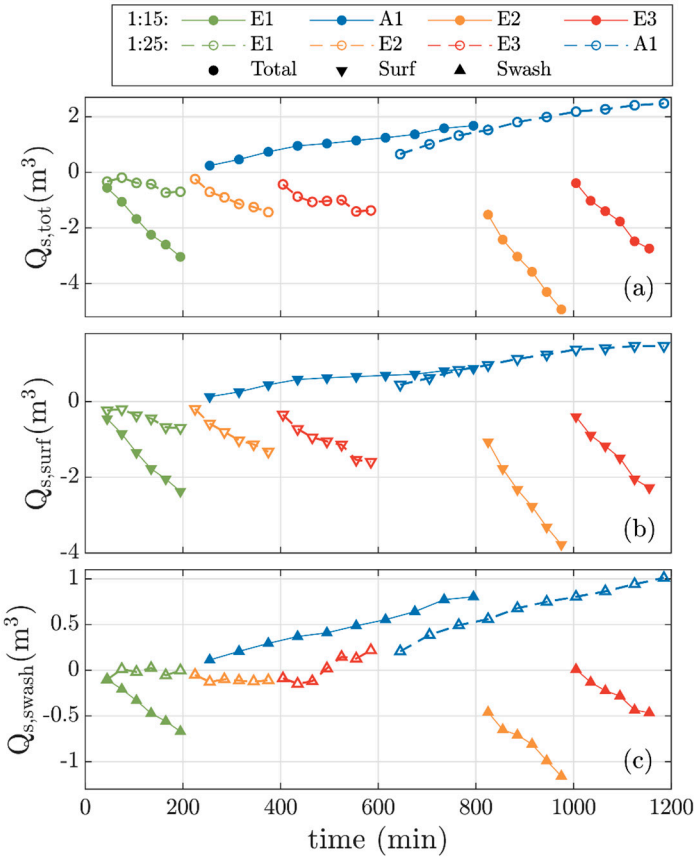

Figure 8. Evolution of the cumulative total bulk cross-shore sediment transport $Q_{s,tot}$ as function of time for each wave condition (**a**), the bulk sediment transport in the surf zone $Q_{s,surf}$ (**b**) and the bulk sediment transport in the swash zone $Q_{s,swash}$ (**c**). Note that the vertical axis limits vary between panels.

The direction and magnitude of the total bulk sediment transport (Figure 8a) for the high-energy wave conditions (E1, E2 and E3) varies in time and per slope. For the 1:15 slope the bulk sediment transport is offshore-directed in all runs of the erosive conditions, reaching the highest magnitudes in the first E2 runs. This supports the idea that the steeper profile at the beginning of E2 is far from its equilibrium state, inducing a greater amount of sediment transport related to the rapid offshore bar migration (Figure 5a) and shoreline erosion (Figure 6) [3,4,44]. Once the beach profile got close to its quasi-equilibrium state in the final E2 runs, with the main bar reaching an overall stable position, the change to a more energetic regime (E3) induced smaller bed level changes and sand transport rates. The total sediment transport for the higher-energy waves (E1, E2 and E3) on the 1:25 slope are of smaller magnitude than on the 1:15 slope. Furthermore, during some E1 and E3 runs the sediment transport in the swash was onshore-directed.

During the low-energy condition A1, the total sediment transport was onshore-directed for both slopes (Figure 8a). However, there was more sediment transported in the first 180 min of this wave condition on the gentle slope, but magnitudes decreased throughout the condition to values similar to those measured for the steeper 1:15 slope. For both slopes, it is possible to see the tendency of Q_s towards a constant value, indicating a quasi-equilibrium condition.

The sediment transport in the surf and swash zones is different in magnitude and direction depending on the bed slope (Figure 8b,c). On the steeper slope, the high-energy erosive waves (E1, E2, and E3) induce offshore-directed transport both in the surf and in the swash zone that reflects the offshore migration of the main bar and shoreline erosion. On the gentler slope, the transport in the surf zone is also offshore-directed but of smaller

magnitude, reaching values close to zero in some runs during E1 and E3 (Figure 8b), corresponding to a relatively slow development of the main bar. However, in the swash zone of the gentler slope the sediment transport for the high-energy erosive wave conditions oscillates around zero. During E1, the sediment transport in the swash is alternately offshore/onshore-directed per run. During conditions E2 and E3, the sediment transport in the swash was offshore-directed in the first 60 min, whilst positive transport rates were dominating towards the end of these wave conditions. The highest energy wave condition (E3) induced the highest, mainly onshore-directed transport in the swash for the 1:25 slope. The positive swash zone sediment transport reflects the berm growth and the shoreline erosion by the beach-face steepening.

A comparison between the bulk sediment transport for each wave condition on different slopes and for the two variations of the Dean parameter is presented in Figure 9. No trend is obtained when linking the bulk sediment transport on different slopes with Ω_D. The same value of Ω_D is associated with substantially different bulk sediment transport for the two different slopes (Figure 9a). However, a clear trend is found for the total bulk sediment transport with the slope-dependent Ω_{HK} parameter (Figure 9b). A maximum onshore-directed transport occurs at small values of Ω_{HK}, i.e., lower energy and gentle slope. For higher values of Ω_{HK}, i.e., increasing wave energy and bed slope, the sediment transport becomes increasingly offshore-directed. Note that the relatively high (low) sediment transport for E2 (E3) for the steeper slope is associated with the initial beach state being far from (close to) its quasi-equilibrium state (as discussed in Sections 3.1.1 and 3.1.2). The transition from net onshore to net offshore total transport at $\Omega_{HK} \approx 0.1$ agrees reasonably well with the threshold value proposed by Hattori and Kawamata [33].

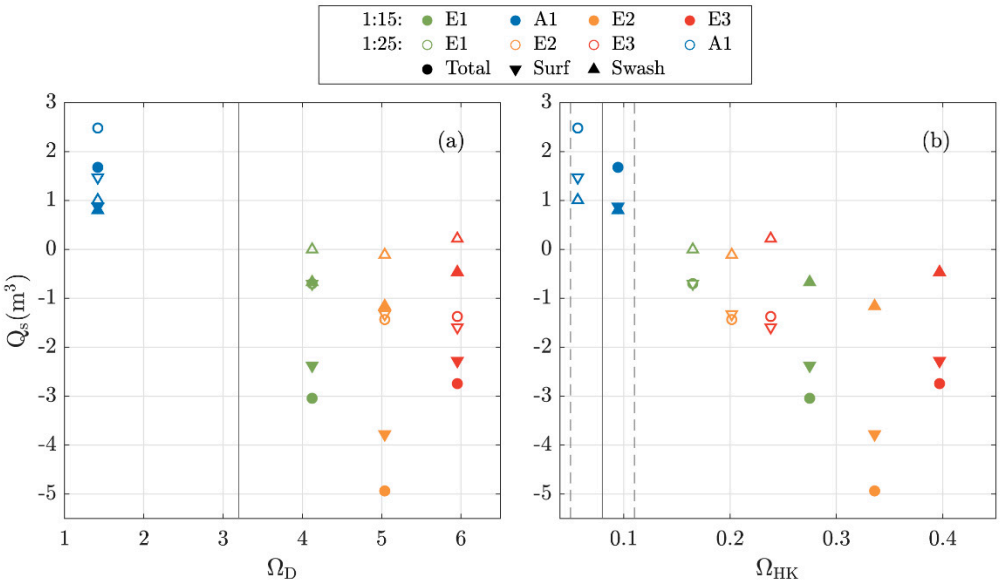

Figure 9. Cumulative bulk sediment transport Q_s for total profile (circles), surf zone (downward-pointing triangles) and swash zone (upward-pointing triangles) against Ω_D (**a**) and Ω_{HK} (**b**) based on bed evolution during each wave condition. Open symbols: 1:25 slope; closed symbols: 1:15 slope. The solid line represents the limits between accretion/erosion for both criteria (mix region within dashed line).

Although a clear relation is observed between the Ω_{HK} and the bulk sediment transport for the total profile and the surf zone, this does not hold for the swash zone sediment transport. The swash zone transport rates were generally onshore-directed for the 1:25 slope (open symbols), even for large Ω_{HK}, while they were offshore-directed for the 1:15 slope. This difference is directly reflected in its contribution to the bulk sediment transport magnitude relative to the surf zone contribution. While for the steep slope both the swash

and surf zone contribute to the offshore-directed total transport, for the gentle slope the onshore-directed transport in the swash zone results into a decrease of the total offshore-directed transport.

3.3. Hydrodynamics and Sediment Transport

Figures 10 and 11 compare hydrodynamic parameters and sediment transport for the last 30 min of wave condition E1 and for the last 60 min of wave condition A1 for both slopes. In order to inter-compare the results for both slopes, the results are presented as function of the slope-corrected cross-shore position $x^* = x\tan(\beta)$ which is a proxy for the local water depth. The hydrodynamics and sediment transport for the higher energetic wave conditions E2 and E3 resulted in similar patterns as shown in Figure 10, but with greater magnitudes in accordance with the respective H_s (Tables 1 and 2). We focus on condition E1 since that followed for both slopes after the same (benchmark) wave condition (Tables 1 and 2).

The sediment transport during wave condition E1 for the 1:15 slope is mainly offshore-directed reaching a peak at the bar crest (Figure 10e,f), remaining offshore-directed until the top of the berm. Wave shoaling occurs on top of the bar (Figure 10a) and is accompanied by an increase in wave skewness and asymmetry (increase of Sk and As, Figure 10c,d) with a peak of As on top of the bar crest. Wave energy dissipation occurs mostly during the breaking over the bar crest with the wave asymmetry reaching its peak in the outer breaking region ($x^* = -0.8$ to -0.5 m). The pronounced breaking induces large amounts of sediment resuspension and a locally strong undertow [46], which combined explain the peak on the offshore-directed transport at $x^* = -0.65$ m. The increasing water depth behind the bar combined with the decreasing wave energy and breaking turbulence induces the decrease in the transport rates at $x^* = -0.5$ m. A new peak in offshore-directed sediment transport is seen again over the secondary bar at $x^* = -0.4$ m. During the shoaling and breaking, the short-wave energy is transferred into long-wave energy that progressively increases up to rundown limit (Figure 10b).

On the 1:25 slope the sediment transport is an order of magnitude smaller than on the 1:15 slope (Figure 10f). Sediment transport is offshore-directed up until the limit between surf and swash at approximately $x^* = -0.2$ m and becomes onshore-directed from that point landward. Thus, the bar generation and migration are driven by an offshore transport (similar to the 1:15 slope), but the bed level changes in the swash zone are driven by onshore transport (gradients). Wave shoaling on the 1:25 slope leads to relatively lower (smaller H_s) and less asymmetric waves compared to the 1:15 slope (Figure 10a,d). In addition, wave breaking occurs over a larger cross-shore distance and leads to a larger wave energy dissipation, as shown by the lower H_s at the surf-swash transition (vertical lines).

Sediment transport in the breaking region is strongly connected to the shoaling and breaking process, which drives onshore wave-related transport, turbulent resuspension, and offshore-directed current-related transport by the undertow [47]. Hence, because waves on the 1:25 slope are lower and less steep, and because breaking and turbulence production occurs over a larger area, both bedload and suspended load transport can be expected to be lower than for the 1:15 slope. This is indeed reflected in the smoother and smaller offshore-directed sediment transport peak over the wider bar for the 1:25 slope as opposed to the pronounced offshore-directed sediment transport peak corresponding to the more localized area of wave breaking over the bar for the steep slope (Figure 10e). Further onshore, as the wave energy decreases, the sediment transport for the 1:25 slope becomes onshore-directed, which is likely due to wave skewness and asymmetry effects. The long waves start becoming more predominant right at the beginning of the outer swash and are relatively more important than for the 1:15 slope (Figure 10b). This agrees with the empirical predictor by Guza and Inman [48] and observations by Hughes et al. [49] in which long-waves become more important in the swash of gentle sloping beaches than for steeper beaches.

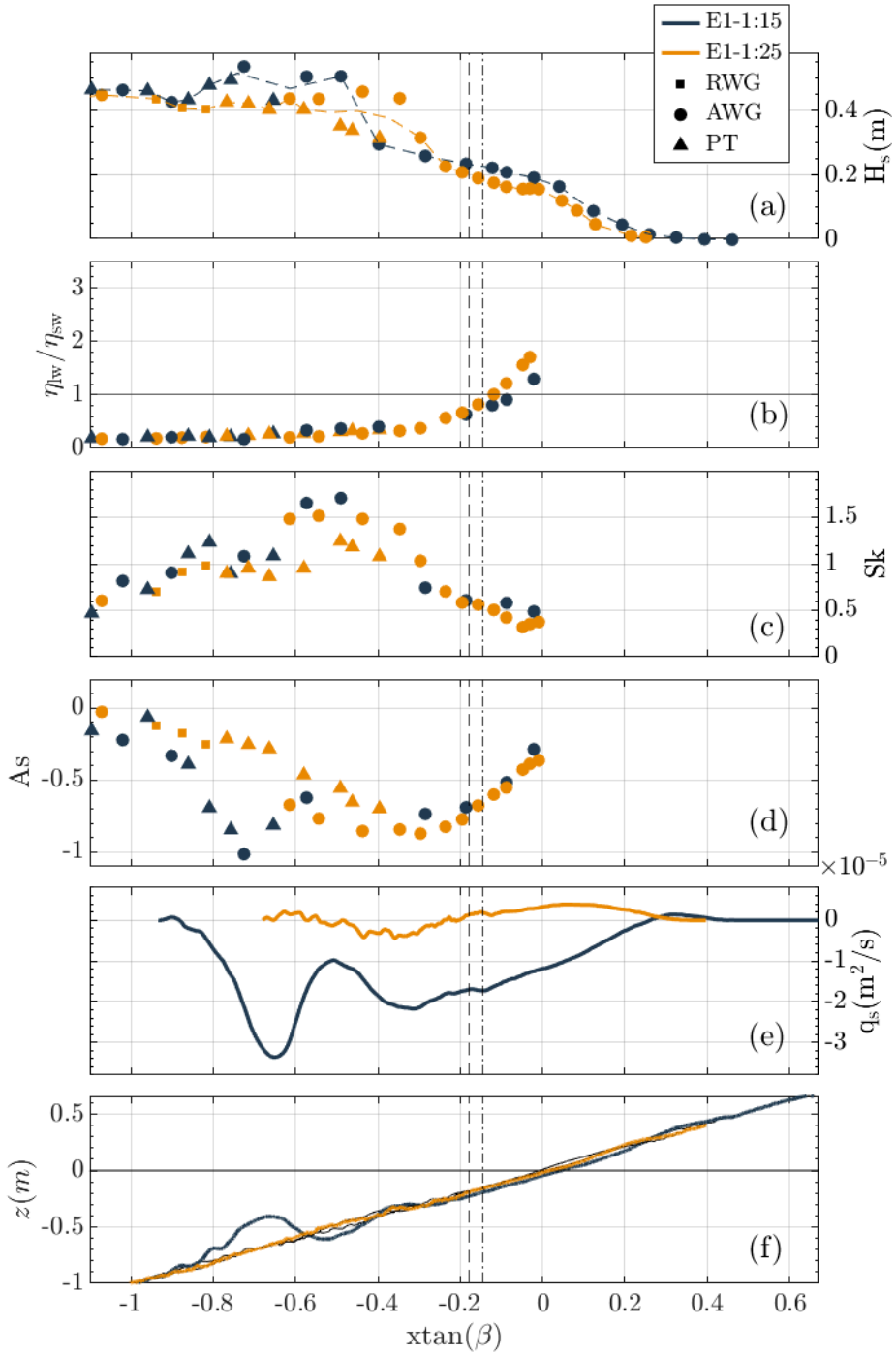

Figure 10. Comparison between the two slopes 1:15 (blue) and 1:25 (red) for the last 30 min of wave condition E1: (**a**) significant wave height H_s, due to overestimation by AWG and underestimation of PPT in the breaking zone a moving average is shown by the dashed line; (**b**) ratio between long-waves and short-waves η_{lw}/η_{sw}; (**c**) wave skewness *Sk*; (**d**) wave asymmetry *As*; (**e**) and sediment transport q_s calculated as the difference between the final and the precedent profile (Δt = 30 min); (**f**) initial profile (black line) and last profile of the wave condition. The vertical lines represent the limit between surf zone and swash zone for the 1:15 slope (dashed black line) and for the 1:25 slope (dashed-dotted black line).

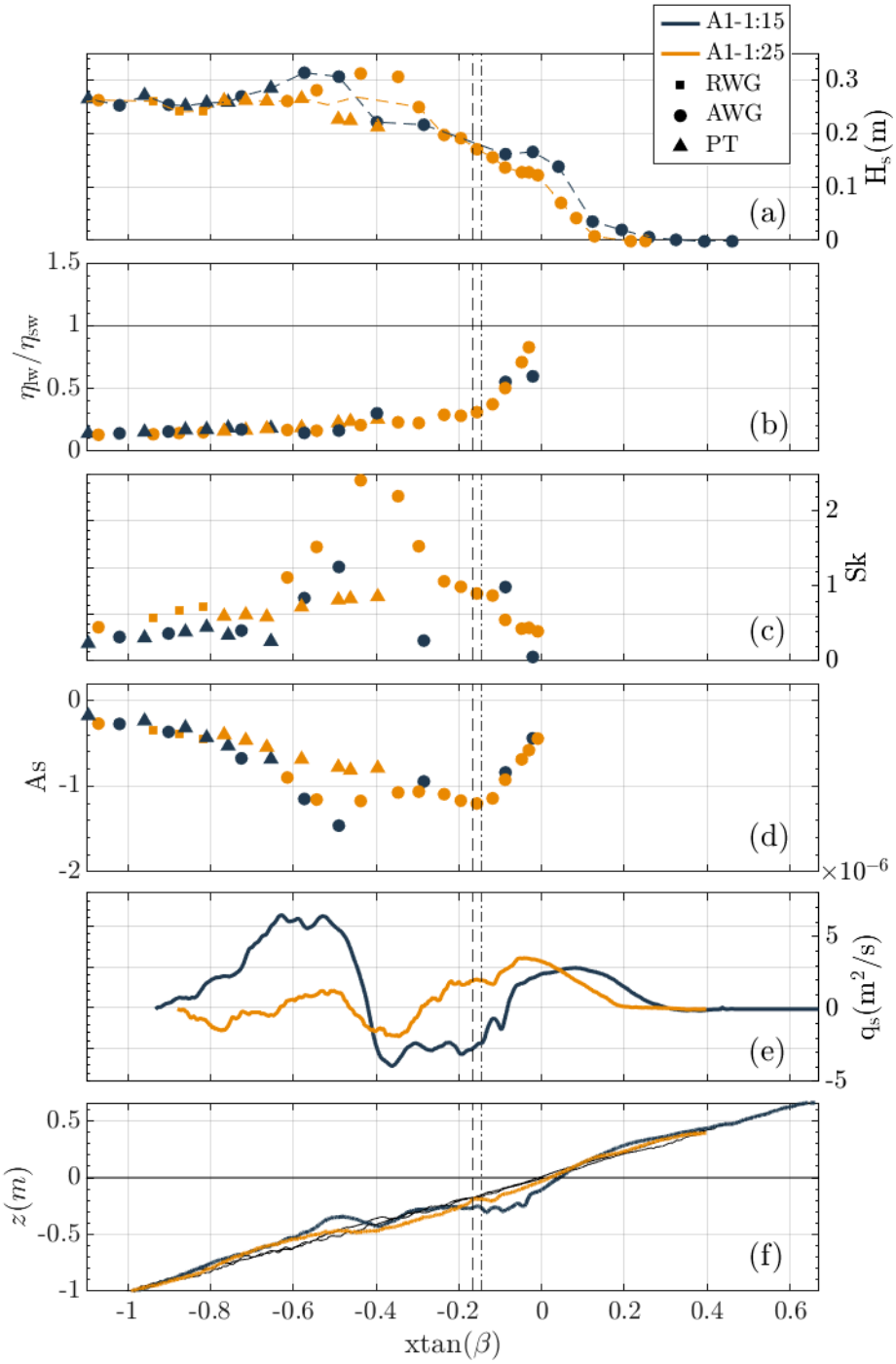

Figure 11. Comparison between the two slopes 1:15 (blue) and 1:25 (red) for the last 60 min of wave condition A1: (**a**) significant wave height H_s due to overestimation by AWG and underestimation of PPT in the breaking zone a moving average is shown by the dashed line; (**b**) ratio between long-waves and short-waves η_{lw}/η_{sw}, (**c**) wave skewness *Sk*; (**d**) wave asymmetry *As*; (**e**) sediment transport q_s calculated as the difference between the final and the precedent profile (Δt = 60 min); (**f**) initial profile (black line) and last profile of the wave condition. The vertical lines represent the limits between surf zone and swash zone for the 1:15 slope (dashed black line) and for the 1:25 slope (dashed-dotted black line).

During the low-energy wave condition A1, the sediment transport for both slopes is mainly onshore-directed and shows a similar pattern, having two positive peaks over the main bar and in the swash zone (Figure 11f). For the 1:15 slope, the sediment transport

reaches its maximum onshore-directed peak at the main bar between $x^* = -0.7$ m and -0.5 m, matching the peak in wave energy, the decrease of *As* and the increase of *Sk* (Figure 11a,c,d). The weak and scarce wave breaking over the breaker bar results in the concentration of wave dissipation in the inner swash. The combination of undertow and the backwashes induces the offshore-directed sediment transport rates, with erosion of the inner swash and filling up of the trough, and the turbulent uprushes contributing to the onshore-directed sediment transport [27]. On the 1:25 slope, although the sediment transport curve generally has a similar pattern as the 1:15 slope, the sediment transport is mainly onshore-directed in the inner surf and swash zone, with the peak over the main bar is considerably smaller (Figure 11e). The absence of a pronounced main bar on the 1:25 slope induced wave shoaling and breaking over a wider cross-shore distances and at a more onshore location in comparison to the 1:15 slope (Figure 11a), resulting in an increase in transfer of short-wave energy to long-wave energy (Figure 11b).

4. Discussion

4.1. Order of the Wave Conditions and Quasi-Equilibrium Profiles

Despite the difference in initial beach profiles between the consecutive runs, the rapid establishment of a quasi-equilibrium state (with relatively small changes in bar dimensions and shoreline position, after large initial adjustments) for high energetic conditions allowed for the comparison of the different dynamics for the two slopes studied. In the present experiments, although the same wave conditions were applied for the two slopes, the increasing wave energy sequence was interrupted by a lower-wave energy (A1) for the 1:15 slope (Table 1) whereas this lower-wave energy was ran after all erosive wave conditions for the 1:25 slope (Table 2). For the steep slope, this led to the largest morphologic changes in the first 90 min of the following wave condition (E2). Independent of the initial beach profile, previous studies have shown that the beach evolves towards the same quasi-equilibrium morphology that is imposed by the wave condition [43–45,50]. The difference between this quasi-equilibrium beach morphology and the initial beach morphology at the change of wave conditions (A1 to E2 in this case) only affects the rates of morphological change and sediment transport, which tend to be larger in the short period following the change in hydrodynamics [45,50]. These rates reduce strongly in the quasi-equilibrium state. For similar experiments as discussed in the present paper, Eichentopf et al. [4] found that for energetic conditions the profile would rapidly evolve into a quasi-equilibrium state, with the main bar reaching a stable position after about 90 min, independent of the initial profile with a slower development of the shoreline. This is consistent with the results from this study (Figures 4 and 5). Consequently, after this initial adaptation period for each of the wave conditions, the morphology and sediment transport on the two slopes can be intercompared, although the E2 condition after 180 min still bears some influence of the initial bed level on the final shoreline position and the cumulative bulk sediment transport (see Figures 6 and 9). Nevertheless, this does not affect the observed relation between bed slopes and beach morphodynamics.

4.2. Beach Recovery under Low-Energy Conditions

Morphological changes towards an equilibrium under low energetic wave conditions are slower than under more energetic conditions [4,51,52]. The underlying mechanisms contributing to this difference are not fully understood. In the present experiments, for both slopes the lower-energy condition (A1) started on a developed profile with a main bar, which favours intercomparison of the general beach behaviour between slopes. Beach recovery, onshore bar migration and shoreline advance occurred in both cases but at different rates (Figures 5 and 6). The bar flattening was followed by a slower onshore migration on the gentler slope, as opposed to the faster onshore bar migration and decay on the steeper slope, suggesting that differences in bed slope influence the main bar morphodynamics. However, even though results in Figure 6 show a greater shoreline advance for the 1:25 slope and an overall arrest of the shoreline for the 1:15 slope, the latter

seems more a local phenomenon controlled by the inner surf/outer swash erosion and the swash berm growth, and not so much directly related to the larger-scale differences in hydrodynamics related to beach slope. During condition A1 for the 1:15 slope the inner surf/outer swash eroded as the result of the energy dissipation closer to the shoreline. The eroded sediment was deposited at the berm, resulting it to increase in height. Combined, these dynamics result in the arrest of the shoreline position. The increase in deepening of the inner surf/outer swash is not only associated to the inner surf breaking turbulence but can also likely be associated with the occurrence of wave–swash interactions which increase the sediment stirring in this area. For the 1:25 slope the steepening of the beach face was not as intense as for the 1:15 slope, associated with the shallower (but wider) trough between the beach and the main bar. Since only one lower-energy wave condition was tested, it is not possible to attribute a clear relation between the beach slope and the overall accretion dynamics of the shoreline. Further investigation is needed to understand the influence of the bed slope on beach recovery under low-energy conditions.

4.3. Morphological Activity

Overall, the morphological development of the gentle beach was substantially slower and less pronounced than for the steep beach, with differences in Δz_0 of the main beach features of about half those for the steeper beach (Figure 7). Furthermore, the steep beach developed into a double-barred system (previously also observed by Baldock et al. [2], Cáceres and Alsina [26], Eichentopf et al. [50]) while for the gentle beach a secondary bar is absent. This suggests that for the same wave conditions, a steep slope induces faster morphologic changes (resulting in a well-formed double-barred system at an early stage) while the gentle slope induces slower morphologic adjustment. This is in line with Jacobsen and Fredsoe [42] who predicted a more active morphological response for steeper beach slopes. The differences between the morphological activity for both slopes can be associated with wave breaking along the profile. While for the steeper slope plunging wave breaking was focused around the two breaker bar locations (Figure 10) (similarly as observed in Eichentopf et al. [4]), for the gentler slope the breaking occurred over a length of approximately 8 m (between $x = -20$ and $x = -11.6$ m) with breaking waves showing characteristics closer to the spilling type. Thus, the more energetic local breaking at the main and secondary bar on the 1:15 slope acted as positive feedback promoting bar development. While on the gentle slope, the shallow depths further offshore induced energy dissipation over an extended area along the profile resulting in less energetic wave breaking which reduced the morphological activity.

4.4. Swash Zone Dynamics

The total sediment transport and the sediment transport in the surf zone correlate with the beach-slope modified Dean parameter by Hattori and Kawamata [33], both in terms of direction and magnitude, with increasing offshore-directed net sand transport (erosion) for increasing wave energy and bed slope (Figure 9). This is in line with findings from Jiménez and Sánchez-Arcilla [34] and Jiménez et al. [53] who argued the importance of including the beach slope in the prediction of direction and magnitude of surf zone sediment transport. However, although the magnitude of sediment transport in the swash zone is lower for the gentler slope than for the steeper slope, the erosion/accretion threshold of $\Omega_{HK} = 0.08$ suggested by Hattori and Kawamata [33] does not fit the onshore-directed sediment transport seen for the high-energy wave conditions on the gentler slope. Nevertheless, this net onshore sediment transport was accompanied by shoreline retreat (Figure 6) which indicates erosion of the shoreface. Thus, while it is possible to attribute a reasonable relation between the Ω_{HK} predictor and the accretion/erosion of the beach, this parameter does not seem to fit as a predictor for the swash zone sand transport. This suggests that swash zone sediment transport cannot be described by the offshore wave conditions, beach slope and sediment fall velocity only.

According to the distribution of wave dissipation along the profile (Figure 10a), wave breaking is concentrated locally at the breaker bars for the steep slope. This induces an increase of energy entering the swash zone compared to the gentler slope where the wave energy was dissipated along the profile. Thus, the amount of wave energy entering the swash is defined by the slope, with more energy for steeper slopes. The higher energy in the swash increases the potential of suspended sediment and sheet flow stirring during the turbulent uprushes and the end of the backwashes, resulting in an increase in sediment transport [12,54].

Both sediment transport magnitude and direction in the swash zone can also be affected by the wave–swash interactions. The turbulence induced by wave–swash interactions results in increasing sediment mobilization and suspended sediment transport. The degree of wave–swash interactions can be quantified by the ratio of the natural period of individual swash events T_s and the incident wave period T through the parameter $\hat{T} = T_s/T$ [25]. The parameter $\hat{T}$ is directly related to bore height H_b and the beach gradient: $\hat{T} \sim H_b/(T\sin\beta)$ [25,55]. Therefore, for the same beach slope, an increase in bore height will induce longer swash periods T_s and therefore larger $\hat{T}$ resulting in a higher number of wave–swash interactions. Analogously, for the same wave condition, a decrease in beach slope will increase the number of wave–swash interactions. For the current experiments, the latter effect seems to prevail. The effect of the bed slope difference is greater than the effect of the difference in incoming bore height. As such, swash periods are longer on the 1:25 slope than on the 1:15 slope resulting in higher number of wave–swash-interactions, but these wave–swash interactions may be less intense and of a weaker type because of the lower level of wave energy, compared to the steeper slope (Figures 10 and 11).

Previous studies have indicated a tendency towards offshore-directed transport for a strong backwash and an onshore-directed transport for weak backwash and wave capture interactions [23,26,56]. Cáceres and Alsina [56] found that the type of interactions is controlled by the long-waves that determine the location and timing at which wave–backwash interactions occur. Long-waves induce longer backwashes, promoting weak-backwash type of interactions, and therefore, promoting onshore-directed transport. Results from Figure 10b show that the ratio between short waves and long waves is slightly greater at the steeper slope than at the gentler slope, indicating the characteristic predominance of long waves in the swash zone of dissipative beaches [11,12]. Thus, our results suggest that there is a greater predominance of weak-backwash swash interactions at the gentler beach, whereas the strong-backwash interactions dominate at the steeper beach. Similarly, Alsina et al. [23] observed a predominance of weak-backwash interactions over strong-backwash interactions for the same wave condition after reshaping the swash zone to a gentler slope. Note that Alsina et al. [23] left the bed in the surf zone and parts further offshore unchanged, unlike the experiments reported in this paper where the slope of the entire profile was modified. This suggests that for gentler swash slopes the predominant sediment transport is onshore-directed, while for steeper swash slopes the transport is predominantly offshore-directed, in line with the swash transport rates presented in Figure 8c.

Besides the controlling processes discussed above, the cross-shore advection of the sediment within the swash zone and between the surf and swash zones could be an important factor [27]. The effect of the bed slope on such sediment advection effects is not well known. Further detailed intra-swash scale investigations are needed to determine the controlling mechanisms, and their relation to the beach slope.

5. Conclusions

The influence of the beach slope on cross-shore beach morphology and sediment transport is studied using experimental data from a large-scale wave flume. Beaches with an initial slope of 1:15 and 1:25 were exposed to two sequences of irregular 3 high-energy erosive wave conditions and 1 low-energy accretive wave condition.

The morphological activity increases with the beach slope, with faster and more pronounced morphological changes and larger sand transport rates at the steeper beach. This

is accompanied by local wave breaking above the well-developed breaker bars, allowing more energy to enter the swash at the steeper beach. The gentler beach slope induced more offshore and spread-out wave energy dissipation, reducing the wave energy entering the shallower swash.

The total (surf + swash) sediment transport rates as well as the transport rates for the surf zone only were offshore-directed for the high-energy wave conditions and onshore-directed for the low-energy wave condition for both slopes. The net swash zone sediment transport was offshore-/onshore-directed for the high-energy waves at the steeper/gentler slope, respectively, and onshore-directed for the low-energy wave condition at both slopes.

The direction and magnitude of the total and surf zone sediment transport correlate well with the modified Dean number $\Omega_{HK,}$ taking into account the beach slope. Increasing offshore net transport (erosion) was observed for increasing wave energy and a steeper slope. This relation did not hold for the high-energy swash zone sediment transport on the 1:25 slope.

Differences in swash zone net transport depend on the bed slope and are likely to be associated with slope-induced differences in incoming wave energy, wave–swash interactions and the relative importance of long- and short-waves.

Author Contributions: S.D.A.: Conceptualization, Methodology, Formal analysis, Investigation, Writing—Original Draft, Visualization. J.v.d.W.: Conceptualization, Methodology, Writing—Review & Editing, Supervision, Funding acquisition. E.H.: Methodology, Writing—Review & Editing, Supervision. I.C.: Methodology, Investigation, Data Curation, Writing—Review & Editing. J.A.: Methodology, Writing—Review & Editing. J.v.d.Z.: Conceptualization, Writing—Review & Editing, Funding acquisition. S.H.: Writing—Review & Editing, Supervision, Project administration, Project acquisition. All authors have read and agreed to the published version of the manuscript.

Funding: The experiments described in this work were part of the Shaping the Beach project (2018–2023) funded by NWO-TTW research project (no. 16130), with in-kind support by Deltares.

Data Availability Statement: The research data used in this paper are available on request to the corresponding author.

Acknowledgments: We thank fellow Shaping the Beach researchers Bart Vermeulen and the CIEM-LAB staff Joaquim Sospedra, Oscar Galeo and Ricardo Torres for their contributions to the experiments. The data supporting the results in this study will be available upon reasonable request after completion of the Shaping the Beach project.

Conflicts of Interest: The authors declare no conflict of interest.

References

1. Alsina, J.M.; Padilla, E.M.; Cáceres, I. Sediment transport and beach profile evolution induced by bi-chromatic wave groups with different group periods. *Coast. Eng.* **2016**, *114*, 325–340. [CrossRef]
2. Baldock, T.E.; Alsina, J.; Caceres, I.; Vicinanza, D.; Contestabile, P.; Power, H.; Sanchez-Arcilla, A. Large-scale experiments on beach profile evolution and surf and swash zone sediment transport induced by long waves, wave groups and random waves. *Coast. Eng.* **2011**, *58*, 214–227. [CrossRef]
3. Baldock, T.E.; Birrien, F.; Atkinson, A.; Shimamoto, T.; Wu, S.; Callaghan, D.; Nielsen, P. Morphological hysteresis in the evolution of beach profiles under sequences of wave climates—Part 1; observations. *Coast. Eng.* **2017**, *128*, 92–105. [CrossRef]
4. Eichentopf, S.; van der Zanden, J.; Cáceres, I.; Baldock, T.E.; Alsina, J.M. Influence of storm sequencing on breaker bar and shoreline evolution in large-scale experiments. *Coast. Eng.* **2020**, *157*, 103659. [CrossRef]
5. Baldock, T.E.; Manoonvoravong, P.; Pham, K.S. Sediment transport and beach morphodynamics induced by free long waves, bound long waves and wave groups. *Coast. Eng.* **2010**, *57*, 898–916. [CrossRef]
6. Grasso, F.; Michallet, H.; Barthélemy, E. Sediment transport associated with morphological beach changes forced by irregular asymmetric, skewed waves. *J. Geophys. Res. Ocean.* **2011**, *116*, C03020. [CrossRef]
7. Kranenborg, J.W.M.; Campmans, G.H.P.; Jacobsen, N.G.; van der Werf, J.J.; Reniers, A.J.H.M.; Hulscher, S.J.M.H. Depth-Resolved Modelling of Intra-Swash Morphodynamics Induced by Solitary Waves. *J. Mar. Sci. Eng.* **2022**, *10*, 1175. [CrossRef]
8. Chen, W.; van der Werf, J.J.; Hulscher, S.J.M.H. A review of practical models of sand transport in the swash zone. *Earth-Sci. Rev.* **2023**, *238*, 104355. [CrossRef]

9. Butt, T.; Evans, D.; Russell, P.; Masselink, G.; Miles, J.; Ganderton, P. An integrative approach to investigating the role of swash in shoreline change. In Proceedings of the 28th International Conference on Coastal Engineering, ASCE, Cardiff, UK, 7–12 July 2002; pp. 917–928.
10. Alsina, J.M.; Cáceres, I. Sediment suspension events in the inner surf and swash zone. Measurements in large-scale and high-energy wave conditions. *Coast. Eng.* **2011**, *58*, 657–670. [CrossRef]
11. Masselink, G.; Evans, D.; Hughes, M.G.; Russell, P. Suspended sediment transport in the swash zone of a dissipative beach. *Mar. Geol.* **2005**, *216*, 169–189. [CrossRef]
12. Miles, J.; Butt, T.; Russell, P. Swash zone sediment dynamics: A comparison of a dissipative and an intermediate beach. *Mar. Geol.* **2006**, *231*, 181–200. [CrossRef]
13. Aagaard, T.; Jensen, S.G. Sediment concentration and vertical mixing under breaking waves. *Mar. Geol.* **2013**, *336*, 146–159. [CrossRef]
14. Aagaard, T.; Hughes, M.G. Sediment suspension and turbulence in the swash zone of dissipative beaches. *Mar. Geol.* **2006**, *228*, 117–135. [CrossRef]
15. Butt, T.; Russell, P.; Puleo, J.; Miles, J.; Masselink, G. The influence of bore turbulence on sediment transport in the swash and inner surf zones. *Cont. Shelf Res.* **2004**, *24*, 757–771. [CrossRef]
16. Flick, R.E.; George, R.A. Turbulence scales in the surf and swash. In Proceedings of the 22nd International Conference on Coastal Engineering, ASCE, Delft, The Netherlands, 2–6 July 1990; pp. 559–569.
17. Battjes, J.A. Surf similarity. In Proceedings of the 14th International Conference Coastal Engineering ASCE, Copenhagen, Denmark, 2–28 June 1974; pp. 1419–1438.
18. Elfrink, B.; Baldock, T. Hydrodynamics and sediment transport in the swash zone: A review and perspectives. *Coast. Eng.* **2002**, *45*, 149–167. [CrossRef]
19. Blenkinsopp, C.E.; Turner, I.; Masselink, G. Russell, PSwash zone sediment fluxes: Field observations. *Coast. Eng.* **2011**, *58*, 28–44. [CrossRef]
20. Masselink, G.; Russell, P.; Turner, I.; Blenkinsopp, C. Net sediment transport and morphological change in the swash zone of a high-energy sandy beach from swash event to tidal cycle time scales. *Mar. Geol.* **2009**, *267*, 18–35. [CrossRef]
21. Puleo, J.A.; Lanckriet, T.; Blenkinsopp, C. Bed level fluctuations in the inner surf and swash zone of a dissipative beach. *Mar. Geol.* **2014**, *349*, 99–112. [CrossRef]
22. Alsina, J.M.; Falchetti, S.; Baldock, T.E. Measurements and modelling of the advection of suspended sediment in the swash zone by solitary waves. *Coast. Eng.* **2009**, *56*, 621–631. [CrossRef]
23. Alsina, J.M.; Cáceres, I.; Brocchini, M.; Baldock, T.E. An experimental study on sediment transport and bed evolution under different swash zone morphological conditions. *Coast. Eng.* **2012**, *68*, 31–43. [CrossRef]
24. Baldock, T.E.; Manoonvoravong, P.; Pham, K.S. Beachface morphology and surf beat sediment transport in laboratory scale surf and swash zones. In Proceedings of the 9th International Coastal Symposium, Gold Coast, QLD, Australia, 16–20 April 2007; pp. 631–635.
25. Brocchini, M.; Baldock, T.E. Recent advances in modeling swash zone dynamics: Influence of surf-swash interaction on nearshore hydrodynamics and morphodynamics. *Rev. Geophys.* **2008**, *46*, 1–21. [CrossRef]
26. Cáceres, I.; Alsina, J.M. A detailed, event-by-event analysis of suspended sediment concentration in the swash zone. *Cont. Shelf Res.* **2012**, *41*, 61–76. [CrossRef]
27. van der Zanden, J.; Cáceres, I.; Eichentopf, S.; Ribberink, J.S.; van der Werf, J.J.; Alsina, J.M. Sand transport processes and bed level changes induced by two alternating laboratory swash events. *Coast. Eng.* **2019**, *152*, 103519. [CrossRef]
28. Baldock, T.E.; Hughes, M.G. Field observations of instantaneous water slopes and horizontal pressure gradients in the swash-zone. *Cont. Shelf Res.* **2006**, *26*, 574–588. [CrossRef]
29. Hughes, M.G.; Moseley, A.S. Hydrokinematic regions within the swash zone. *Cont. Shelf Res.* **2007**, *27*, 2000–2013. [CrossRef]
30. Masselink, G.; Russell, P. Flow velocities, sediment transport and morphological change in the swash zone of two contrasting beaches. *Mar. Geol.* **2006**, *227*, 227–240. [CrossRef]
31. Dalrymple, R.A. Prediction of Storm/Normal Beach Profiles. *J. Waterw. Port Coast. Ocean. Eng.* **1992**, *118*, 193–200. [CrossRef]
32. Dean, R.G. Heuristic models of sand transport in the surf zone. In Proceedings of the 1st Australian Conference on Coastal Engineering, Engineering Dynamics of the Coastal Zone, Sydney, NSW, Australia, 14–17 May 1973; pp. 215–221.
33. Hattori, M.; Kawamata, R. Onshore-Offshore Transport and Beach Profile Change. In Proceedings of the 17th International Coastal Engineering Conference, Sydney, NSW, Australia, 23–28 March 1980; pp. 1175–1193. [CrossRef]
34. Jiménez, J.A.; Sánchez-Arcilla, A. Simulación de cambios a corto plazo en la línea de costa. *Rev. Obras Públicas* **1992**, *139*, 41–51.
35. Kraus, N.C.; Larson, M. *Beach Profile Change Measured in the Tank for Large Waves: 1956–1957 and 1962*; Technical Report CERC-88-6; Coastal Engineering Research Center (U.S.): Ft. Belvoir, VA, USA, 1988.
36. Kraus, N.C.; Larson, M.; Kriebel, D.L. Evaluation of Beach Erosion and Accretion Predictors. In Proceedings of the Coastal Sediments '91. ASCE, Seattle, WA, USA, 25–27 June 1991; pp. 572–587.
37. Eichentopf, S.; Baldock, T.E.; Cáceres, I.; Hurther, D.; Karunarathna, H.; Postacchini, M.; Ranieri, N.; van der Zanden, J.; Alsina, J.M. Influence of storm sequencing and beach REcovery on SedIment TranSporT and beach resilience (RESIST). In Proceedings of the HYDRALAB+ Joint User Meeting, Bucharest, Romania, 23 May 2019; pp. 1–9.

38. Masselink, G.; Ruju, A.; Conley, D.; Turner, I.; Ruessink, G.; Matias, A.; Thompson, C.; Castelle, B.; Puleo, J.; Citerone, V.; et al. Large-scale Barrier Dynamics Experiment II (BARDEX II): Experimental design, instrumentation, test program, and data set. *Coast. Eng.* **2016**, *113*, 3–18. [CrossRef]
39. Bonneton, P.; Lannes, D.; Martins, K.; Michallet, H. A nonlinear weakly dispersive method for recovering the elevation of irrotational surface waves from pressure measurements. *Coast. Eng.* **2018**, *138*, 1–8. [CrossRef]
40. van Thiel de Vries, J.S.M. *Dune Erosion during Storm Surges*; Delft University of Technology: Delft, The Netherlands, 2009; p. 202.
41. Jacobsen, N.G.; Fredsoe, J.; Jensen, J.H. Formation and development of a breaker bar under regular waves. Part 1: Model description and hydrodynamics. *Coast. Eng.* **2014**, *88*, 182–193. [CrossRef]
42. Jacobsen, N.G.; Fredsoe, J. Formation and development of a breaker bar under regular waves. Part 2: Sediment transport and morphology. *Coast. Eng.* **2014**, *88*, 55–68. [CrossRef]
43. Pape, L.; Plant, N.G.; Ruessink, B.G. On cross-shore migration and equilibrium states of nearshore sandbars. *J. Geophys. Res. Earth Surf.* **2010**, *115*, 1–16. [CrossRef]
44. Wright, L.D.; Short, A.D.; Green, M.O. Short-term changes in the morphodynamic states of beaches and surf zones: An empirical predictive model. *Mar. Geol.* **1985**, *62*, 339–364. [CrossRef]
45. Yates, M.L.; Guza, R.T.; O'Reilly, W.C. Equilibrium shoreline response: Observations and modeling. *J. Geophys. Res. Ocean.* **2009**, *114*, 1–16. [CrossRef]
46. van der Zanden, J.; Hurther, D.; Cáceres, I.; O'donoghue, T.; Ribberink, J.S. Suspended sediment transport around a large-scale laboratory breaker bar. *Coast. Eng.* **2017**, *125*, 51–69. [CrossRef]
47. van der Zanden, J.; Hurther, D.; Cáceres, I.; O'Donoghue, T.; Hulscher, S.J.; Ribberink, J.S. Bedload and suspended load contributions to breaker bar morphodynamics. *Coast. Eng.* **2017**, *129*, 74–92. [CrossRef]
48. Guza, R.T.; Inman, D.L. Edge waves and beach cusps. *J. Geophys. Res.* **1975**, *80*, 2997–3012. [CrossRef]
49. Hughes, M.G.; Aagaard, T.; Baldock, T.E.; Power, H.E. Spectral signatures for swash on reflective, intermediate and dissipative beaches. *Mar. Geol.* **2014**, *355*, 88–97. [CrossRef]
50. Eichentopf, S.; van der Zanden, J.; Cáceres, I.; Alsina, J.M. Beach profile evolution towards equilibrium from varying initial morphologies. *J. Mar. Sci. Eng.* **2019**, *7*, 406. [CrossRef]
51. Maspataud, A.; MRuz, H.; Hequette, A. Spatial variability in post-storm beach recovery along a macrotidal Barred beach, Southern North Sea. *J. Coast. Res.* **2009**, *I*, 88–92.
52. Ranasinghe, R.; Holman, R.; de Schipper, M.; Lippmann, T.; Wehof, J.; Duong, T.M.; Roelvink, D.; Stive, M. Quantifiying Nearshore Morphological Recovery Time Scales Using ARGUS Video Imaging: Palm Beach, Sydney and Duck, North Carolina. In Proceedings of the 33rd International Conference on Coastal Engineering, Santander, Spain, 1–6 July 2012; pp. 1–7.
53. Jiménez, J.A.; Sánchez-Arcilla, A.; Stive, M.J.F. Discussion "Prediction of Storm/Normal Beach Profiles". *J. Waterw. Port Coast. Ocean. Eng.* **1993**, *119*, 466–468. [CrossRef]
54. Masselink, G.; Puleo, J.A. Swash-zone morphodynamics. *Cont. Shelf Res.* **2006**, *26*, 661–680. [CrossRef]
55. Baldock, T.E.; Holmes, P. Simulation and prediction of swash oscillations on a steep beach. *Coast. Eng.* **1999**, *36*, 219–242. [CrossRef]
56. Cáceres, I.; Alsina, J.M. Suspended sediment transport and beach dynamics induced by monochromatic conditions, long waves and wave groups. *Coast. Eng.* **2016**, *108*, 36–55. [CrossRef]